ORIGINAL ARTICLE

Processing, mechanical characterization, and micrography of 3D-printed short carbon fiber reinforced polycarbonate polymer matrix composite material

Ankit Gupta[1] · Ismail Fidan[2] · Seymur Hasanov[1] · Aslan Nasirov[1]

Abstract

The objective of this research is to perform the processing and mechanical characterization on 3D-printed high-temperature polymer (polycarbonate) reinforced with short carbon fiber (SCF) composite material fabricated with the help of fused filament fabrication process. For this study, different SCF volume fractions (3%, 5%, 7.5%, 10%) with varying printing speed (25, 50, 75 mm/s) are taken as the input variables. It was observed that tensile, flexural, compressive properties and micro-hardness were greatly affected by varying the input processing parameters. To find the orthotropic properties of 3D-printed specimens, tensile properties are analyzed on 0° in the X-Y plane, 90° in the X-Y plane, and 90° in Z-axis. Scanning electron microscopy (SEM) is performed to study the effect of fiber breakage, fiber distribution, fiber accumulation, and fiber length on the mechanical performance of the final part. After performing mechanical testing, investigation of microstructural behavior of tensile, flexural, and compressive samples is accomplished using SEM. From the micrograph analysis and mechanical testing, it was noticed that fiber behavior inside the composite has created a great influence in deciding the mechanical performance of the final part. Micromechanics and classical lamination theory phenomena are followed to determine the effective young's modulus of 3D-printed samples mathematically. Printing direction and reinforcement percentage are found out to be the most influential parameters in deciding the final properties of 3D-printed specimens by using the statistical tool ANOVA. Response surface methodology is used to determine the optimum parameters to get good-quality print with SCF-reinforced PC.

Keywords Short carbon fiber · Orthotropic · Fused filament fabrication · Composite material · ANOVA · Polycarbonate

✉ Ismail Fidan
  ifidan@tntech.edu

  Ankit Gupta
  agupta42@students.tntech.edu

  Seymur Hasanov
  shasanov42@students.tntech.edu

  Aslan Nasirov
  anasirov42@students.tntech.edu

[1] Department of Mechanical Engineering and Center for Manufacturing Research, Tennessee Technological University, Cookeville, TN, USA

[2] Department of Manufacturing and Engineering Technology, Tennessee Technological University, Cookeville, TN, USA

1 Introduction

Additive manufacturing (AM) is defined as the technology used to create the three-dimensional objects with the help of layer-upon-layer addition of materials like metals, polymers, concrete, ceramics, etc. 3D-printing, layered manufacturing, and rapid prototyping are some of the subsets of AM. As the layers are adding layer-upon-layer, there are many diverse needs that can be fulfilled with this technology like industrial tooling, customizing the products for consumers, small lots of production parts, design flexibility, etc [1]. The advantages of AM are its weight reduction, fewer efforts for assembly, less lead times, no added cost, and the capability of producing the complex parts [2]. Fused deposition modeling (FDM) [3], selective laser melting (SLM) [4], stereolithography apparatus (SLA) [5], and selective laser sintering (SLS) [6] are some of the well-known AM techniques. There are some applications that require properties that cannot be fulfilled by a single material. For those applications, fiber-reinforced additive

manufacturing (FRAM) comes into the picture. FRAM process is quite popular in several industries nowadays [7]. FRAM offers various solutions to these problems as it combines the flexibility of AM and the advantages of composite material (CM). Conventional production of fiber-reinforced products is tedious and costly as all of them require molds which makes the fabrication process costly and also reduces the formability of the final part [8]. Good fiber-matrix bonding, fiber alignment, minimal porosity, and good interlayer bonding are some of the requirements that need to be fulfilled by fiber-reinforced products in order to get processed by AM [8]. The reinforcement in the FRAM process can either be continuous fibers, long fibers, or short fibers depending upon the requirement of the application. Short fibers are extensively used in most of the engineering applications for polymers such as the interior of automobiles, electrical goods, and durable items for consumers because of its easy processing, low cost, and improved mechanical properties over the unreinforced polymer. It is also comparatively inexpensive to produce large-scale CM parts with short fiber-reinforced AM rather than the continuous fiber reinforcement.

Most of the studies only focus on using the fused filament fabrication (FFF) process with single thermoplastic materials like polylactic acid (PLA), acrylonitrile butadiene styrene (ABS), nylon, etc. Limited studies have been reported to develop the thermoplastic CM reinforced with fiber through single-extruder 3D printers. Hofstatter et al. conducted the experiments using extrusion techniques and VAT polymerization (using liquid photopolymer resin as a vat) to enhance the understanding of fiber-reinforced AM. The study focusses on increasing the matrix-fiber adhesion to avoid the delamination and internal cracks. The authors reported that fiber reinforcement helps in increasing in Young's modulus but a decrease in tensile strength and break strength. Improvement in the fiber-matrix interface is required to further enhance the mechanical properties and reduce the failures of the fabricated part [9]. Rezaei et al. investigated the thermomechanical properties of the SCF-reinforced polypropylene (PP) processed with hot pressing techniques and melt blending. The results of this study showed that with the increase in the fiber length, the thermal stability of the CM was improved as compared to neat PP [10]. Yi et al. presented the phenomena related to the transport of four neighboring droplets with the help of experimental and numerical modeling using droplet-based 3D printing. The authors also observed that using the proper droplet and substrate temperatures, hole defects can be eliminated [11]. Lu et al. have used the SLA technique to fabricate the SCF-reinforced SiC ceramics CM and observed the influence of SCF on fracture strength and fracture toughness. The authors analyzed that both the properties showed an increase with the increase of SCF [12]. Jiang et al. performed the experiments on near-α Ti alloy (TA15) using the SLM technique to analyze the part before and after the annealing process. The results of

the study concluded that both the annealed and as-built specimens showed the anisotropic mechanical properties and weak textures, but the annealed samples exhibited a significant improvement in the properties after annealing [13]. Ma et al. performed the SLM printing on Cu–Cr–Zr alloy and analyzed the volume fraction and cell size effect on the final mechanical properties of the printed part [14]. Lehua et al. investigated the droplet-based 3D strategies for dissolvable supports for inclined corners and surfaces [15].

Thomas et al. performed the 3D printing to produce the custom test parts by taking the ABS material reinforced with multiwalled carbon nanotubes. The results showed the enhancement in mechanical strength and electrical conductivity of the final part [16]. Imeri et al. analyzed the effect of fiber orientation, fiber materials (carbon, glass, and Kevlar), and infill type on the fatigue behavior of FRAM samples. The study concluded that high resistance to failure was observed in the case of carbon fiber with zero and one concentric ring (shells around the printed part) [17]. Ferriera et al. performed the mechanical characterization of PLA-reinforced SCF (15% wt. fraction) fabricated with the help of the FDM process. The study reported that short fiber reinforcement showed an increase in young's modulus but did not vary the tensile strength because of the too-short fiber length [18]. Zhong et al. performed the experimental study to find out the influence of short glass fibers on the ABS polymer using the FDM process. [19]. Ivey et al. performed the 3D printing on PLA reinforced with SCF to study the effect of annealing on the mechanical properties of 3D-printed parts. The study showed that there is an increase in elastic modulus after the SCF reinforcement and that annealing helps to improve the crystallinity of the part but did not provide any significant effect on the final mechanical performance [20]. Tekinalp et al. used the AM technique to investigate the mechanical performance, processability, and microstructure of 3D-printed short fiber (0.2–0.4 mm)-reinforced ABS and compared the results with compression molded technique. From this study, authors determined that fibers are more oriented in printing direction in case of 3D-printed parts as compared to compression molded parts. Moreover, despite the presence of porosity inside the 3D-printed parts, tensile strength and modulus are comparable to compression molded parts [21].

Sedighi et al. have investigated the influence of layer orientation on flexural, tensile, and fracture behavior of PC, manufactured using FDM. The results of this study concluded that the layer orientation creates a significant impact on the anisotropy behavior of all the testing specimens [22]. Kumar et al. has performed 3D printing on PC/ABS composite material to increase the mechanical properties as compared to neat PC and ABS. The results of this study showed that with the increase in PC concentration, hardness and strength increases because of good compatibility formation between the two polymers [23].

The study presented here deals with the use of the FFF process for the generation of SCF (dia. 7.2 μm, length 150 μm)-reinforced high-temperature PC matrix composite materials with the help of single-feeder, single-nozzle 3D printing. Mechanical characterization and surface morphology of short carbon fiber-reinforced polycarbonate composite material was performed by observing the distribution of fibers, fiber length, fiber breakage, the orientation of fibers, and interaction area of fiber with the polycarbonate matrix material and gives this research a novelty from other researches. Moreover, through the literature review, it has been found that no mechanical characterization and surface morphology is performed on PC reinforced with SCF polymer matrix composite by considering the influence of process parameters like SCF percentage (3%, 5%, 7.5%, and 10% (by vol.)) and printing speed (25 mm/s, 50 mm/s, 75 mm/s). Bead-to-bead and then layer-by-layer stack-up of CM leads to an orthotropic behavior of the final part. So, this work also presents the testing and analyzing of the material behavior in all the directions, i.e., in the direction of printing (0° in the X-Y plane), perpendicular to the direction of printing (90° in the X-Y plane and 90° in Z-axis). Flexural strength and flexural modulus, compressive strength and compressive modulus, and finally microhardness have been found to determine the ability of 3D-printed composite sample in bending forces. The 3D-printed tensile, flexural, and compression samples were also analyzed by SEM to observe the behavior of the fibers inside the PC. Finally, statistical analysis was performed on the tensile properties for different orientation, variable SCF concentration, and printing speed. ANOVA was performed to find out the most influential process parameter and their interaction for deciding the final mechanical performance of the CM. Response surface methodology (RSM) was performed for determining the optimum process parameters for 3D printing the SCF-reinforced PC to get the maximum tensile properties.

2 Materials and methods

2.1 Experimental setup

In order to make the polymer matrix composite (PMC) reinforced with short fibers, the single-nozzle 3D printer (ULTIMAKER3, 3D UNIVERSE) was used. Table 1 shows the 3D printer processing parameters and were adjusted by performing the number of pilot experiments on PC/SCF filaments. The entire setup from raw material to finished product is schematically shown in Fig. 1.

The setup includes the low-temperature furnace, filament extruder with 2.85 mm diameter hardened steel nozzle head, air path, filament spooler, and finally 3D printer with closed-chamber assembly. The low-temperature furnace was used to dry the PC pellets and SCF before using them for filament

Table 1 3D printing processing parameters

Properties	Values
Bed temperature (°C)	107
Extrusion temperature (°C)	270
Infill density (%)	100
Infill pattern	Line
Closed chamber temperature (°C)	50
Layer thickness (mm)	0.2
Printing speed (mm/s)	25, 50, 75

production. Otherwise, the adsorbed moisture inside the SCF and PC pellets forms bubbles during extrusion from the hot end that creates defects and decreases the surface quality of the final part. Uniform diameter can be achievable by adjusting the filament extruding parameters like extrusion temperature, extrusion speed and air path fan speed as shown in Table 2.

2.2 Effect of the closed chamber

Closed chamber temperature is also considered to be an important parameter while using the PC material in the FDM process. The materials like PC undergo warping when cured (cooled) from high temperatures. After reinforcing the SCF, the effect of warping has occurred in a huge manner because of different thermal expansion and contraction of two different materials. Figure 2 shows the warping behavior of PC/SCF composite material after 3D printing without or with the use of a closed chamber.

This warping of PC/SCF concluded that not only the heating bed and nozzle temperature creates a significant impact on the final print quality and final mechanical properties; the temperature surrounding the 3D printer also has great influence. The closed chamber was specially made for printing PC/SCF for maintaining 50 °C temperature inside the chamber with the help of heater. This helped us to resolve many problems: (**a**) warping of composite material after curing (**b**) keeps the humidity away from the material which attracts the water, (**c**) increases the layer adhesion, and reduces the layer delamination by maintaining the steady temperature around the printer.

2.3 Material selection

To perform the 3D printing of CM, PC pellets from 3DXTECH were used as matrix material and short carbon fibers (SCF) from ZOLTEK as reinforcements. Properties like heat resistance, flame retardant, and electrical insulator properties of PC make it useful for electronic components, lightweight, high impact resistance, high toughness, strong, durable, sustainable for automotive, and optically transparent for medical applications. PC can be easily
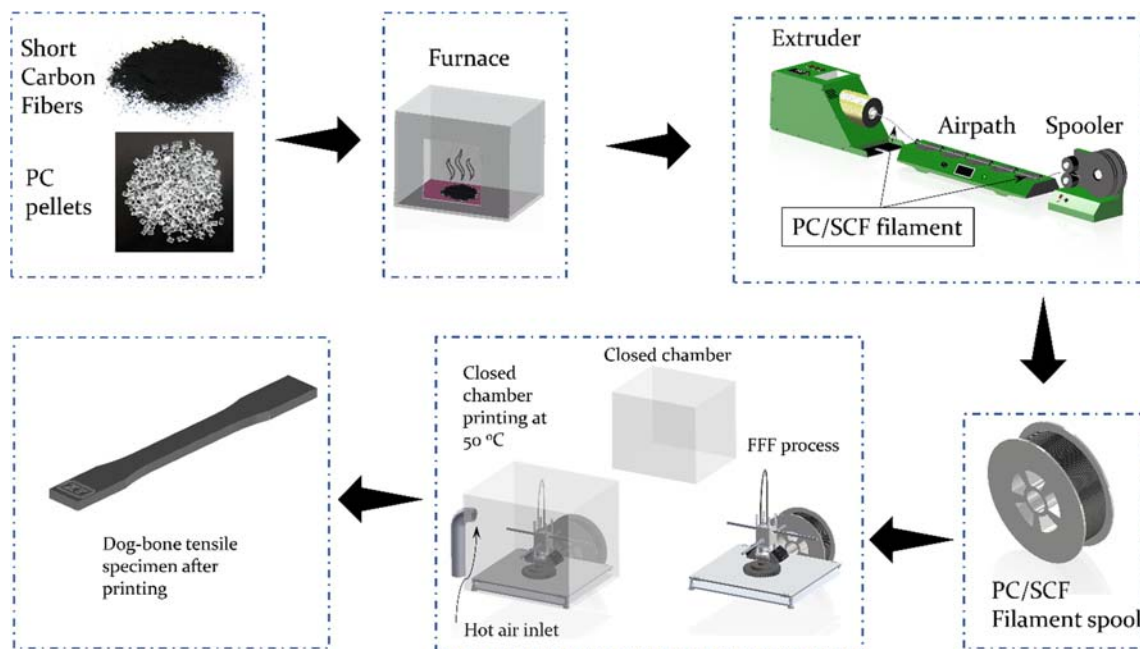
Fig. 1 Schematic view of producing SCF/PC composite material using the 3D printing process

molded and thermoformed allowing its use in the 3D printing process. In order to enhance the mechanical performance of PC and to widen its application, SCF was reinforced inside PC. Carbon fibers (CFs) were used to have high tensile strength, high stiffness, high-temperature tolerance, low thermal expansion, and low weight. This makes the CF as useful fillers in CM manufacturing. Short fibers were used in this research because it helps matrix to encase all the fibers from all the directions to achieve a significant increase in the properties. SCF is very easy to manufacture, easily available, and low cost and can be used in almost all the polymers and allow them to mold into any complex shapes which are not possible with continuous carbon fibers. SCF reinforcement inside the PC helped to increase the strength, stiffness, and hardness of overall composite material which makes it useful in applications like car bonnet [24], wind turbines, lightweight automotive products, armor, satellite components, etc.. Typical PC and SCF properties are shown in Table 3 [25].

2.4 Material mixture preparation

For the formation of PMC, two materials PC and SCF (diameter = 7.2 μm and length = 150 μm) were taken. To determine the amount of fibers, $V_{critical}$ was calculated.

Fiber critical volume fraction ($V_{critical}$) is defined as the value above which the reinforcement starts working for enhancing the properties of CM. It is calculated mathematically with the help of the Eq. (1) [26]:

$$V_{critical} = (Um - fm)/(Uf - fm) \qquad (1)$$

where Um, Uf, and fm are the ultimate tensile strength (UTS) of the matrix, UTS of fiber, and stress carried by matrix at fiber failure strain, respectively. If the load is applied to the CM and the amount of fibers is less than $V_{critical}$, then stresses inside the CM might be high enough to break the fibers and then the extra load is transferred to the matrix material which makes the matrix fail. The net effect is that the strength of CM is even less than the matrix [26]. After performing the tensile test on PC/SCF dog bone specimen and considering Eq. (1), the failure strain of CF is found out to be less than the PC. So, in this study, fiber volume fraction should be taken above 1% in order to take the benefit of fibers inside the CM.

2.5 Experimental procedure

In all the experiments, SCF was used as the reinforced material in high-temperature PC polymer. Four different types of material mixtures were prepared using PC and SCF: (1) 97% PC + 3% SCF (by vol.), (2) 95% PC + 5% SCF (by vol.), (3)

Table 2 Filament extrusion processing parameters

Properties	Values
Extrusion temperature (°C)	270
Air path speed (m/s)	30
Extrusion speed (mm/s)	25
Filament diameter (mm)	2.65 mm – 2.85 mm

Fig. 2 PC/SCF specimens printed using **a** no closed chamber **b** closed chamber

92.5% PC + 7.5% SCF (by vol.), and (4) 90% PC + 10% SCF (by vol.). All the mixtures were allowed to dry in low-temperature furnace for 2 h at 90 °C to get rid of moisture. These dried mixtures were then poured into the hopper of the filament extruder. The single screw extruder was allowed to heat up to 270 °C in order to get the smooth filament to come out from the 2.85-mm hardened steel nozzle. The closed chamber was also allowed to heat up to 50 °C before starting the 3D printing process. Then, the printer accesses the G-code and starts heating the nozzle head for melting the composite filament fed by two-wheel drive and travels in the X-Y plane on the build platform to print the desired specimen's bead by bead and then layer by layer as shown in Fig. 3. 3D printing processing parameters are shown in Table 1. The entire process was repeated for all the specimens to print according to the design of experiments mentioned in Table 4.

3 Results and discussions

Firstly, the number of pilot experiments was performed to check the feasibility of printing the SCF with high-temperature polymer (PC). SEM analysis was performed to check the adhesion of these materials at the interface. Poor adhesion results in the weakening of the entire CM and would

Table 3 Polycarbonate and short carbon fibers properties

Properties	Values	
	Polycarbonate	Short carbon fibers
Melting Point (°C)	270	> 1000
Density (g/cm^3)	1.21	1.81
Longitudinal tensile strength (MPa)	58.24	4137
Glass transition temperature (°C)	140	–
Young's modulus (GPa)	2.57	242
Compressive strength (MPa)	60.45	–
Hardness (MPa)	76.59	–
Flexural strength (MPa)	79.565	–
Thermal conductivity (W/m-K)	0.19–0.22	119–165

not help in increasing the mechanical properties of the final part. It also leads to less working life of 3D-printed specimens. Figure 4 shows SEM images at the interface of PC and SCF (5% by vol.) used. From the images, it is very easy to observe that there is a good adhesion between the materials used. Mechanical testing performed after this also helped to investigate that the bonds created between PC and SCF are strong enough to produce the 3D-printed part with improved mechanical properties.

3.1 Microstructure analysis

After the 3D printing process, SEM analysis was performed by printing the samples with dimensions 10 mm × 10 mm × 10 mm and were cut from two sections with the help of a diamond saw cutter to view them from side or cross-section. The cut samples were polished by using emery papers having grit size ranging from 400 to 600 [27] and then lapping was done using the diamond paste slurry of 0.3 μm particle size [28]. Polymers are the soft materials, which make the PC to flow over the carbon fibers while cutting. In order to remove the PC layer over the carbon fibers, potassium permanganate etching was performed. The etching was done using reagents (sulfuric acid 50 ml, orthophosphoric acid 20 ml, distilled water 5 ml and potassium permanganate 0.55 g) for 15–20 min. Figure 5 shows the microstructure characterization of fabricated PMC by SEM. From the images, we can clearly observe that all the SCFs are uniformly distributed inside the PC matrix with insignificant gaps at the interface which helps in improving the overall mechanical properties (tensile strength, compressive strength, flexural strength, and hardness) of the final part.

3.2 Analysis of tensile properties

3.2.1 Longitudinal tensile strength and modulus of elasticity

The tensile behavior of the 3D-printed composite parts was analyzed with the help of the universal testing machine (UTM—INSTRON 5582) using ASTM tensile test methods. Dog bone sample according to the ASTM D638 [29] standard
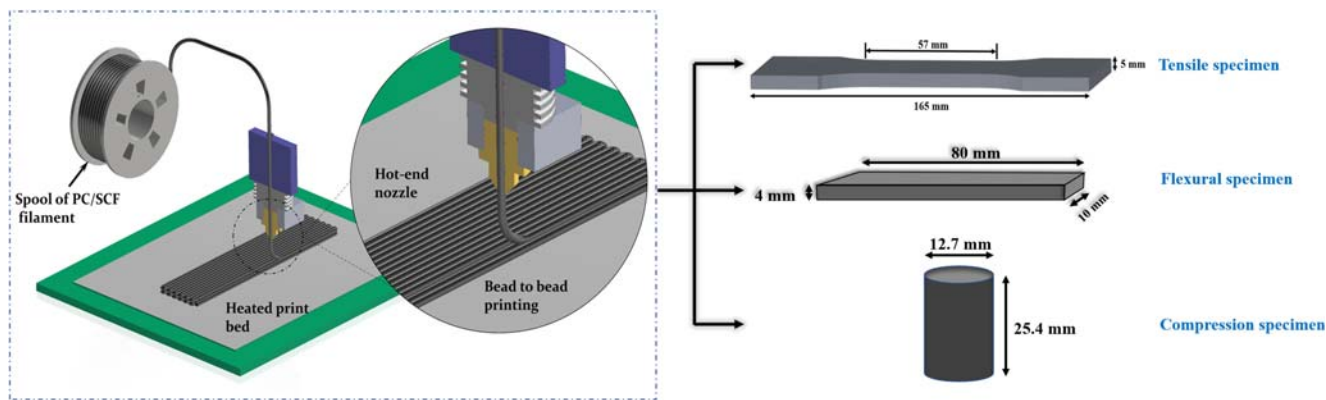
Fig. 3 Bead-to-bead 3D printing process and final testing samples

shown in Fig. 3 was used to get the tensile properties like tensile strength, Young's modulus, toughness, and ductility. For each experimental parameter, three samples were printed and tested with a strain rate of 5 mm/min and a gauge length of 50 mm. The entire procedure was performed at ambient temperature (25 °C).

3.2.2 Reinforcement effect

Samples were printed in 0° in the X-Y plane by varying printing speed and SCF concentration, and the load was applied uniaxially to investigate the changes in strength and modulus. Figure 6 shows the tensile samples for pure PC and reinforced PC after testing. As we are applying the load in printing direction, fibers will decide the overall strength, stiffness, and other properties. The tensile strength of the 3D-printed CM increases as we increase the reinforcement percentage. The reason for this is due to a more uniform distribution of SCF inside the PC as shown in Fig. 5 which eventually results in uniform distribution of load from the matrix to fibers:

Table 4 Different experimental 3D printing parameters

S. No	Reinforcement (% by vol.)	Printing speed (mm/s)
1.	3%	25
2.		50
3.		75
4.	5%	25
5.		50
6.		75
7.	7.5%	25
8.		50
9.		75
10.	10%	25
11.		50
12.		75

$$\frac{P_f}{P_m} = \frac{E_f}{E_m} \times \frac{V_f}{V_m} \tag{2}$$

P_f, P_m tensile load in the direction of fibers and matrix (N)

E_f, E_m Young's modulus of carbon fiber and PC respectively (GPa)

V_f, V_m carbon fiber and PC percentage inside the CM

The mathematical formula is shown in Eq. (2), derived assuming that fibers and matrix material are bonded perfectly so that the strain rate between them could be the same. So, the above mathematical analyses stated that as we increase the volume fraction of SCF in the PC matrix, the fibers started taking more load, i.e., load transfer between the matrix and fiber increases. This increase was noticed by up to 7.5% SCF and as we further increase the concentration, the tensile strength started decreasing or tries to get a stable value as shown in Fig. 7b. The decrement in strength beyond 7.5% has occurred because the fibers start accumulating in one place as shown in Fig. 8b and PC might find it difficult to flow between all the fibers and stick with the fibers to transfer load. So, there are a lot of areas in the CM which might remain dry and ultimately results in decreasing the strength of the CM. In the case of a higher percentage of fibers, the fiber pullout shown in Fig. 8c and fiber breakage in Fig. 8d are also more, creating greater number of voids which result in decreasing the strength.

Table 5 shows the variation in fiber length with an increase in the reinforcement. The composite filament was heated at 800 °C to degrade the polymer material and then the length of the left-out fibers was measured. This decrease in the fiber length is observed due to fiber breakage while extruding and 3D printing the composite filament. This breakage occurs due to shear stress formation created by a single screw inside the extruder to the carbon fibers.
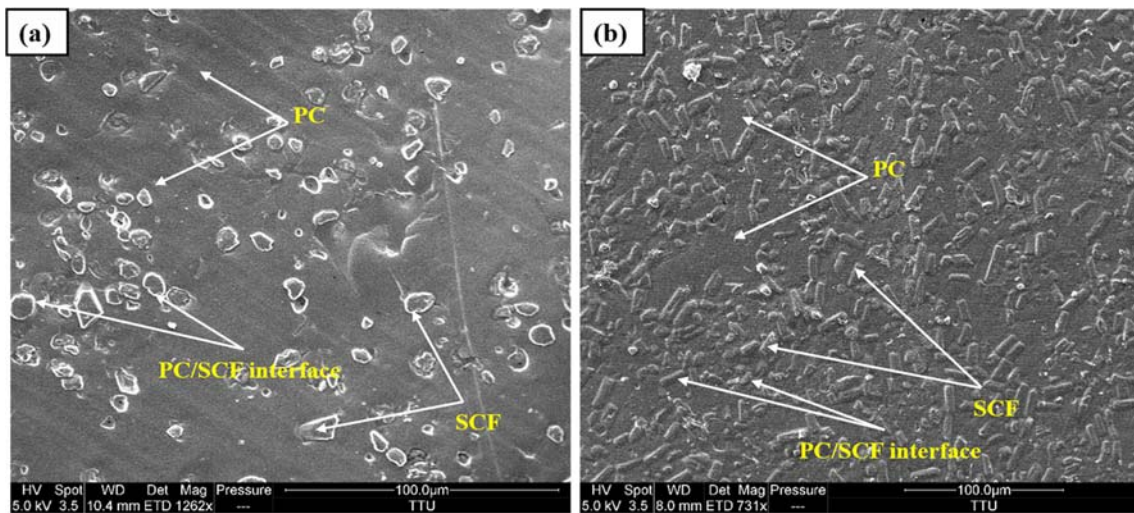
Fig. 4 SEM images showing the insignificant gaps at the interface for SCF (5% by vol)/PC

Moreover, during the filament generation process and 3D printing, the composite material has to pass through the nozzle with a very little orifice which makes the fibers interact and abrade each other. Although the pure PC has more tensile strength as compared to reinforced one, the maximum strength achieved for reinforced CM is 96.6% of the pure PC. The reason behind it is that the SCFs are not perfectly aligned inside the PC, and they all are aligned at
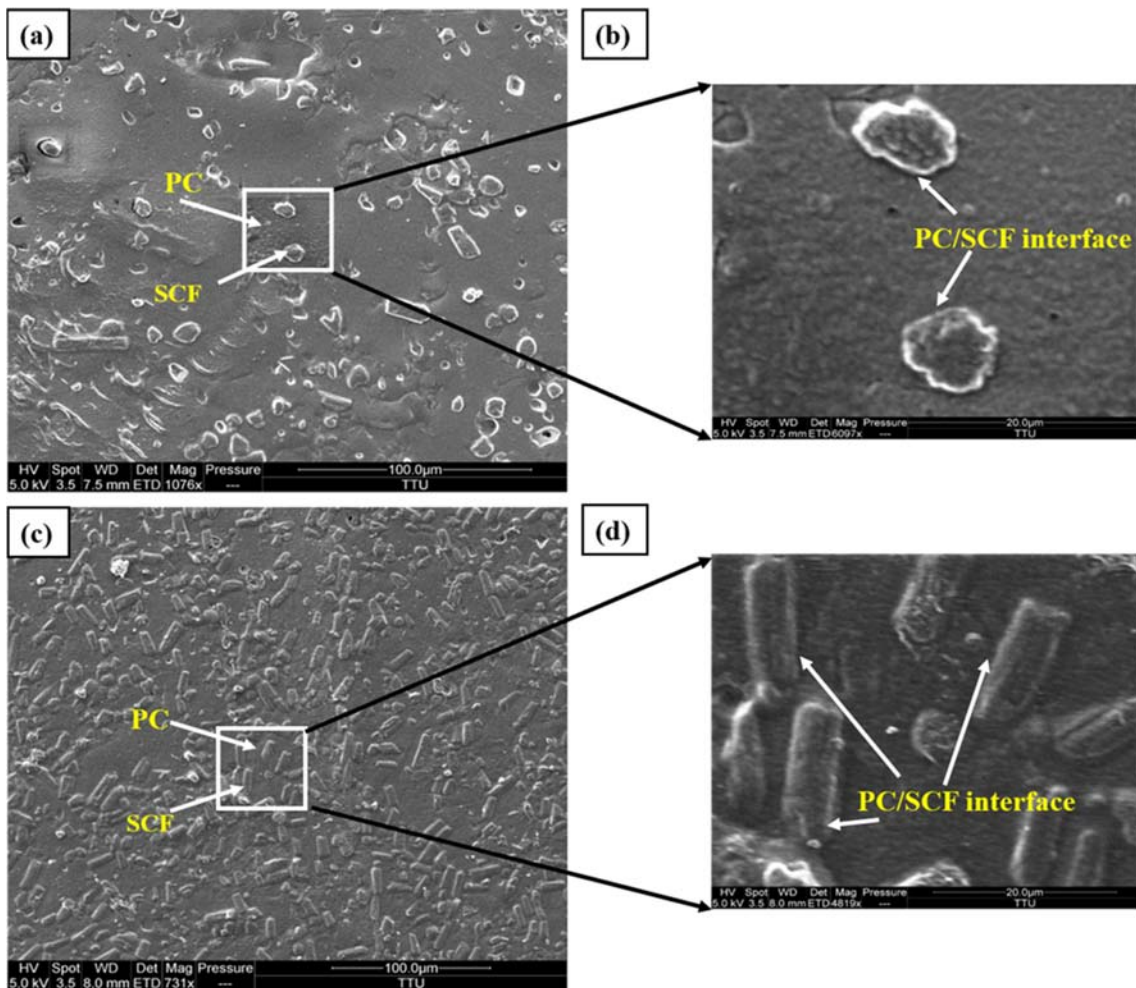
Fig. 5 SEM images showing the uniform distribution of SCF (5% by vol.) inside the PC matrix

Fig. 6 Dog bone samples for longitudinal tensile properties after tensile testing
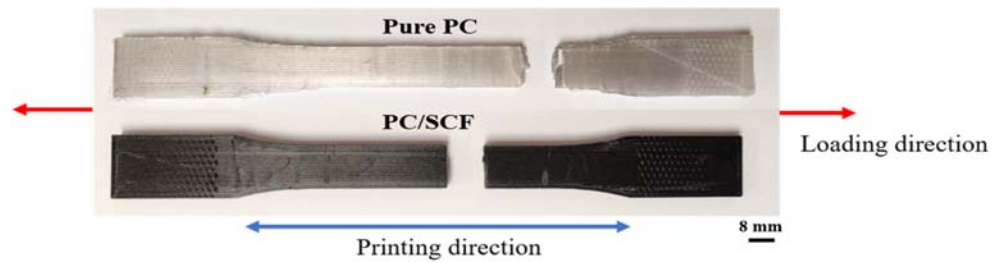
some angle as shown in Fig. 5. So, as we applied the load in one direction, the fibers themselves act as a stress concentrator which eventually increases the local stress inside the material. The stress concentration is more at the fiber ends and usually propagates at the matrix-fiber interface and results in premature failure or matrix cracking.

In most of the CM, fibers are stiffer than the matrix. Because of that, they restrain the movement of the polymer chains in the vicinity of other chains which ultimately increases the stiffness values of the entire CM. The same thing happened in the case of SCF reinforced PC as shown in Fig.

7c. The maximum modulus of elasticity of reinforced CM is 248.16% of the pure PC.

3.2.3 Effect of printing speed

Printing speed plays an important role in making the part with the best finish and good adhesion. Strength and modulus both decrease as we keep on increasing the printing speed as shown in Fig. 7b, c. Maximum improvement in mechanical properties was achieved at the speed of 25 mm/s. As we increase the speed, polymer might get less time in the melting zone to melt
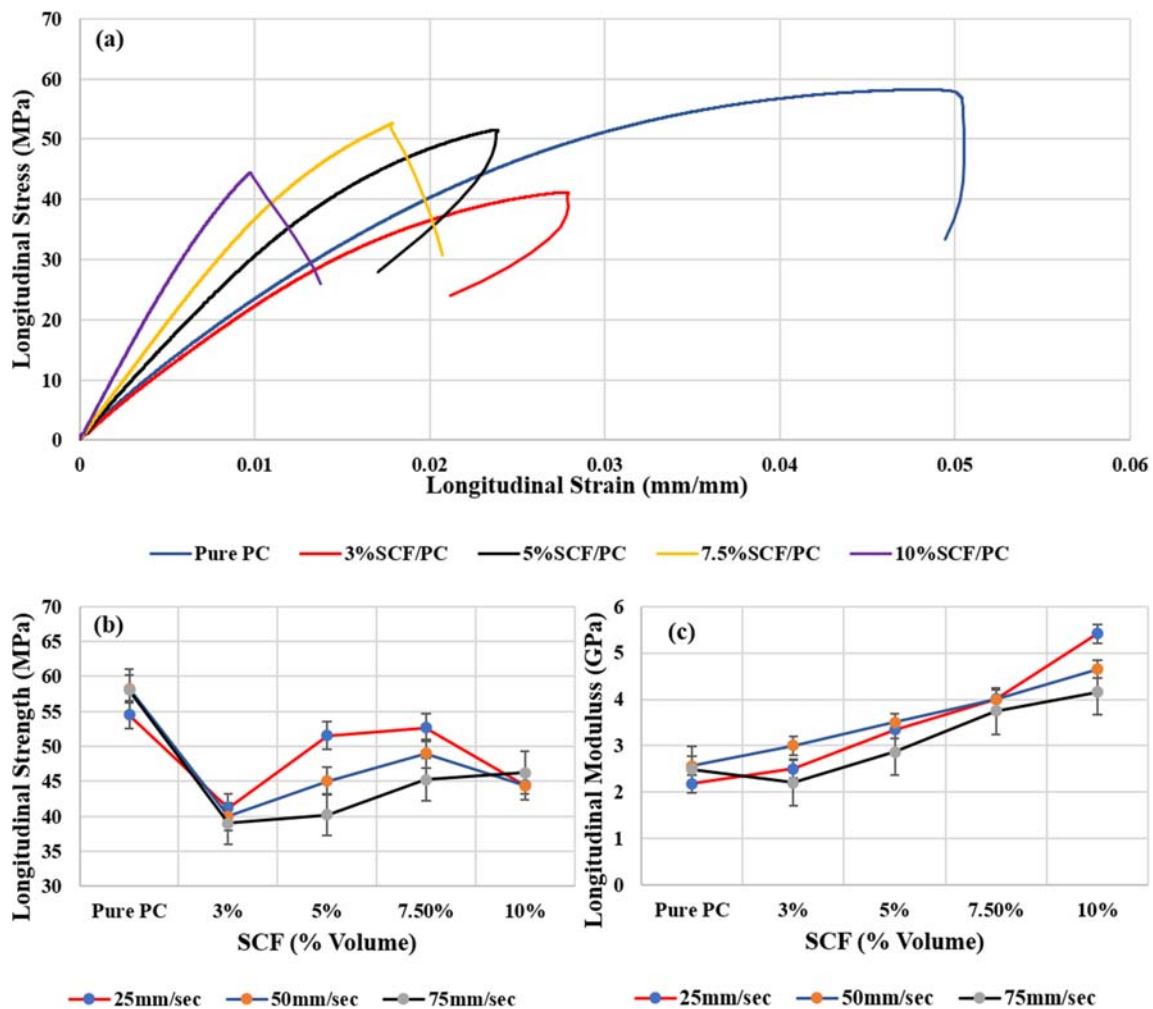

Fig. 7 a Longitudinal stress-strain curve for all SCF percentage. **b** Effect of SCF percentage on longitudinal strength at printing speed of (i) 25 mm/s, (ii) 50 mm/s, (iii) 75 mm/s. **c** Effect of SCF percentage on longitudinal modulus at printing speed of (i) 25 mm/s, (ii) 50 mm/s, (iii) 75 mm/s
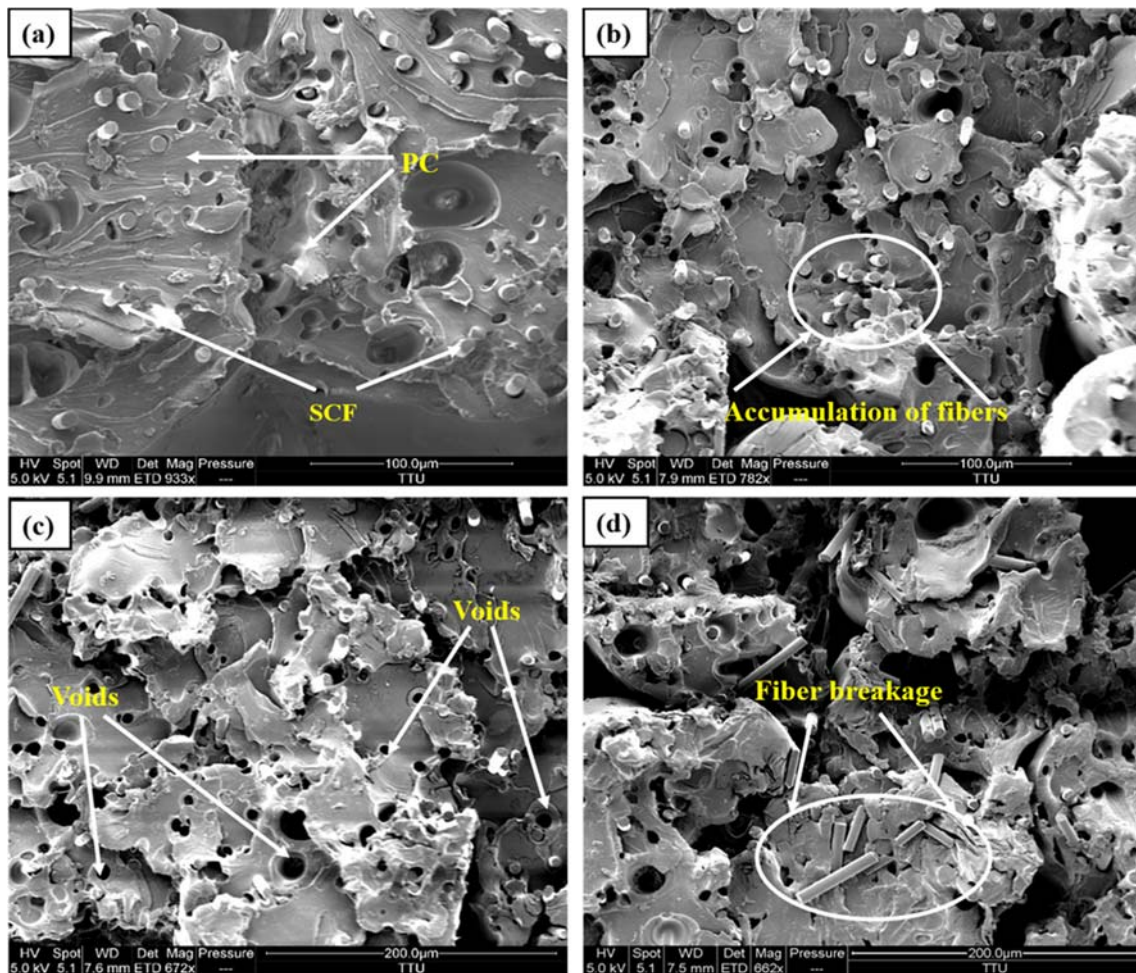
Fig. 8 SEM images of samples after tensile testing. **a** Distribution of fibers and matrix. **b** Accumulation of fibers at one place. **c** Fiber pull out at high percentage. **d** Fiber breakage

properly which deteriorates the mechanical performance and surface finish of the final part.

3.2.4 Transverse tensile strength and modulus

The CM reinforced with SCF fabricated with the FFF process is a highly anisotropic material. Usually, the CM's are fabricated to be loaded along the longitudinal or high strength direction. Although, transverse loads are also present in-service applications, so needs to be evaluated. To fully

Table 5 Fiber length variation after 3D printing extrusion process for different concentration

S. no.	Reinforcement (% by vol.)	Average length (microns)
1.	3	118.142
2.	5	95.916
3.	7.5	55.066
4.	10	53.866

characterize the part in transverse loading, samples were printed with 90° in the X-Y plane and 90° in Z-axis.

To find out the transverse strength and modulus, the ASTM D638 [29] samples were subjected to load normal to the printing direction or direction of fibers as shown in Fig. 9a. As samples are pulled normal to printing direction, the matrix creates a strong influence in deciding the overall transverse properties of CM. Figure 9 b shows the stress concentration lines generated after applying the load to the sample which makes the fiber inclusions as the stress concentrators. These local stresses distributed at the matrix-fiber interface and decrease the overall transverse strength of fabricated CM as shown in Fig. 10b.

As in the current research, SCFs are used which creates more fiber ends inside the CM. Local stress formations are more pronounced at then fiber ends which ultimately decreases the transverse properties of the CM as compared to longitudinal properties as shown in Fig. 11.

Change in Young's modulus is not significant as we increase the SCF percentage as shown in Fig. 10c because the influence of PC is more as we stretch the sample in the

Fig. 9 Dog bone samples for transverse tensile properties after tensile testing
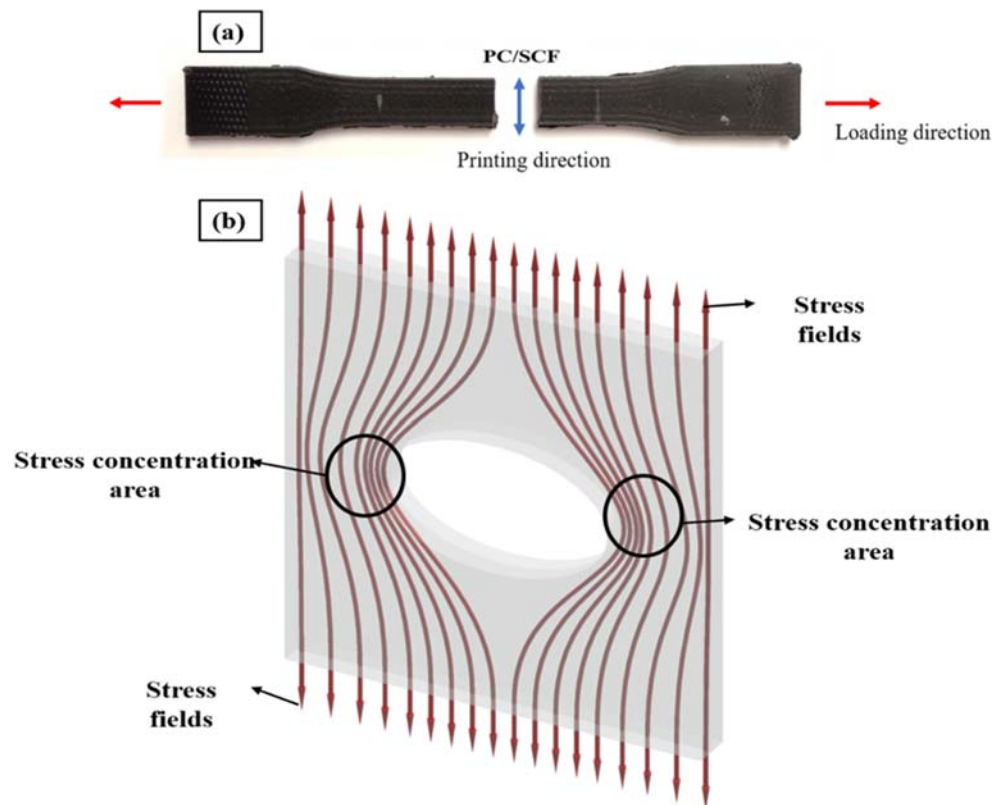
transverse direction. A 19.375% increase in Young's modulus is achieved in the case of transverse tensile load. Transverse properties also showed a decrease with an increase in printing speed as explained in Sect. 3.2.3.

In conclusion, specimens printed with 0° orientation (see Fig. 6) are stronger than samples printed in 90° direction (see Fig. 9a) in terms of both strength and modulus as indicated in Fig. 12. The maximum longitudinal strength achieved is 52.68 MPa which is 27.18% and 144.73% more than the transverse strength in the Y and Z direction respectively. The maximum longitudinal modulus achieved is 5.41 GPa which is 114.68% and 203.08% more than the transverse modulus in the Y and Z direction respectively.

3.2.5 Toughness and ductility

The influence of SCF percentage on ductility and toughness behavior of PC/SCF CM is observed and shown in Fig. 13. Both ductility and toughness decrease with an increase in SCF. As we increase the SCF, the plastic zone of the stress-strain diagram reduces. Breaking strain of CM reduces from approx. 5 to 2%, leading to a low value of ductility and toughness. This happens because the SCF acts as an inclusion inside the PC which results in stress formation. These local stresses initiate the crack formation when load is applied. As the load increases, crack propagation occurs and links up with other cracks in proximity

resulting in a brittle fracture as shown in Figs. 6 and 9a. Generally, the brittle fracture is considered to be the main characteristic of low toughness and ductility.

3.3 Analysis of flexural properties

The flexural properties of the PC/SCF composite were measured with the help of a three-point bending test as per ISO 178 [29] using universal testing machine with specimens of dimensions 80 mm × 10 mm × 4 mm shown in Fig. 3. A minimum of three specimens was tested for each case. The change in the flexural strength and flexural modulus was investigated by varying the printing speed and SCF percentage. Due to increasing demand for product durability, quality, and reliability, these two values can be used to determine the ability of the sample to withstand the bending forces which are most important in research and development and manufacturing domains. The test was performed until the rupture occurred at the outer layer of the specimens. Under this testing procedure, the force applied to the specimens was measured. The flexural stress was calculated from the load data using the following Eq. (3):

$$S = \frac{3PL}{2bd^2} \tag{3}$$

S—stress in the outer surface at a midpoint (MPa), *P*—Load at the given point on the load-deflection curve (N), *L*—support
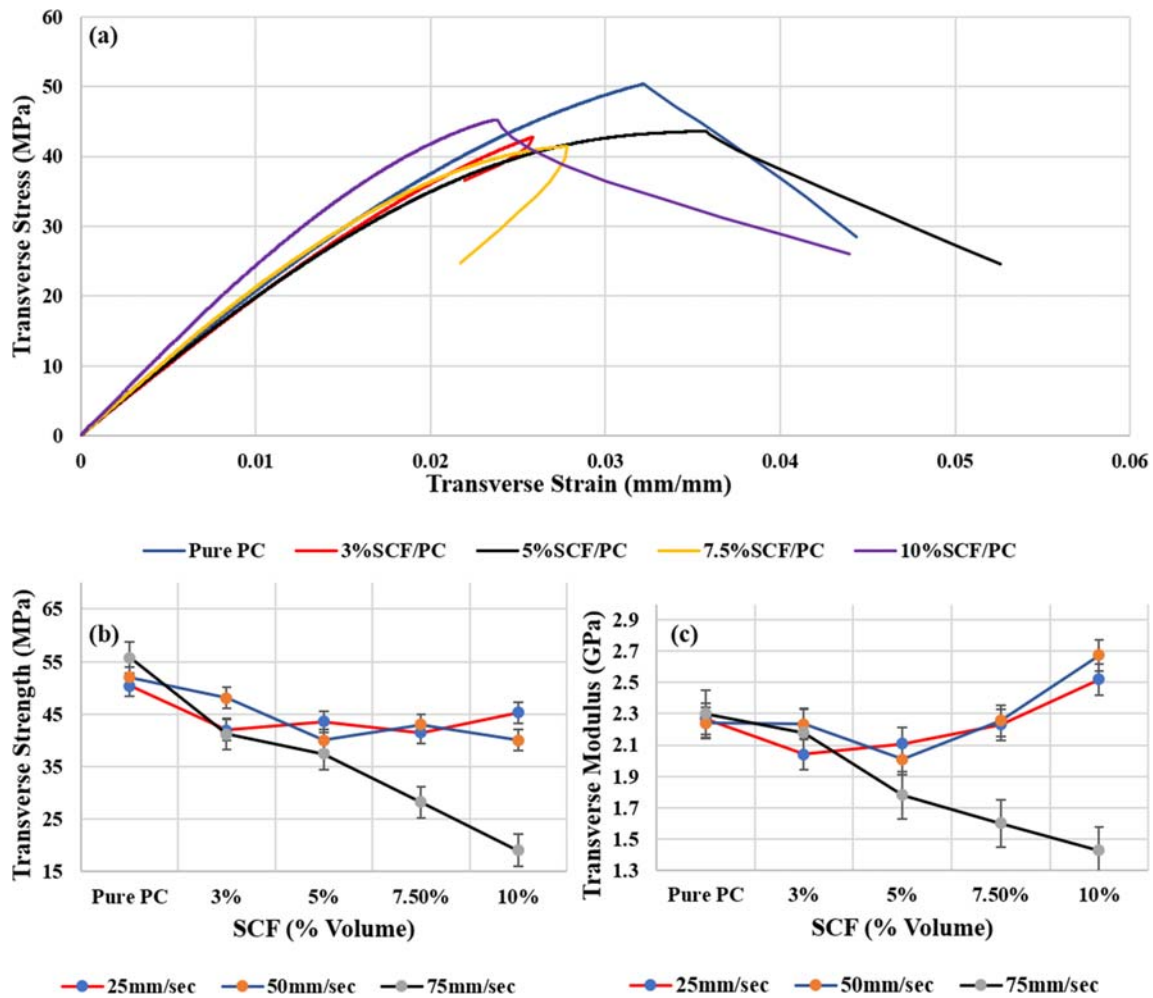
Fig. 10 **a** Transverse stress-strain curve for all SCF percentage. **b** Effect of SCF percentage on transverse strength at printing speed of (i) 25 mm/s, (ii) 50 mm/s, (iii) 75 mm/s. **c** Effect of SCF percentage on transverse modulus at printing speed of (i) 25 mm/s, (ii) 50 mm/s, (iii) 75 mm/s

span (mm), b—width of the specimen (mm), d—thickness of the specimen (mm). Change in the length of the outer surface of the specimen was also observed at the midspan, and this is the point where maximum strain occurs. The strain was also calculated with the following Eq. (4) for any deflection:

$$e = \frac{6Dd}{L^2} \qquad (4)$$

e—flexural strain in the outer surface (mm/mm), and D—maximum deflection at the midspan (mm).

The flexural test performed on PC/SCF showed that when the load was applied to the flexural specimen, the specimen experiences a compressive force at the top surface and tensile forces at the bottom resulting in failure as shown in Fig. 14a. The printing speed was not creating a significant effect on the flexural properties as created by SCF percentage. The flexural strength and modulus increase as the reinforcement value increases as shown in Fig. 15a, b. The significant increase in the strength and modulus is observed due to strong adhesion between the

fiber and matrix and plies as well as explained in Sect. 3.1. Strong fusion results in increasing the mechanical interlocking which ultimately increases the frictional force between the SCF and PC under compressive load. Although voids are also observed on the surface of sample after testing, they are less in amount to create any effect on the final mechanical properties.

3.4 Analysis of compressive properties

A compression test was performed by considering the cylindrical specimen of PC/SCF. The specimen was printed according to ASTM D695 [29] as shown in Fig. 3. The axial strain was calculated by accounting the change in height of specimen, and axial stress was determined by recording axial load during the test. The load cell of 2 KN was used during the experiment at a strain rate of 0.05 in/min (Fig. 16) [30].

Micro-buckling of fibers, fiber kinking, fiber-matrix splitting and delamination are the main failure mechanisms in the compression testing of fiber-reinforced CM. So, in order to

Fig. 11 Stress-strain curve for PC reinforced with 7.5% (by vol.) SCF at 0° in the X-Y plane, 90° in the X-Y plane, 90° in Z-axis
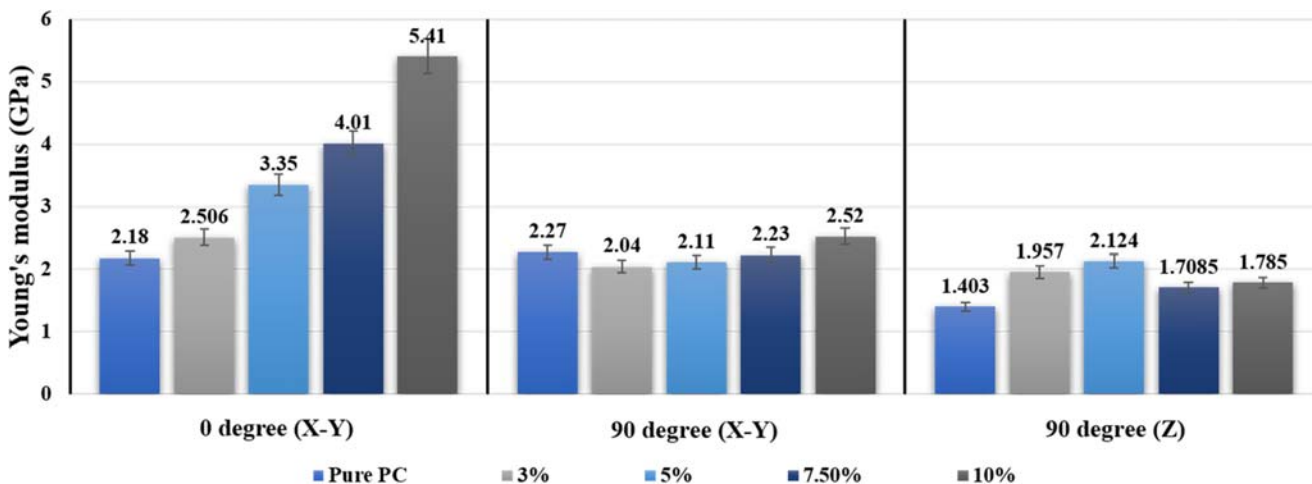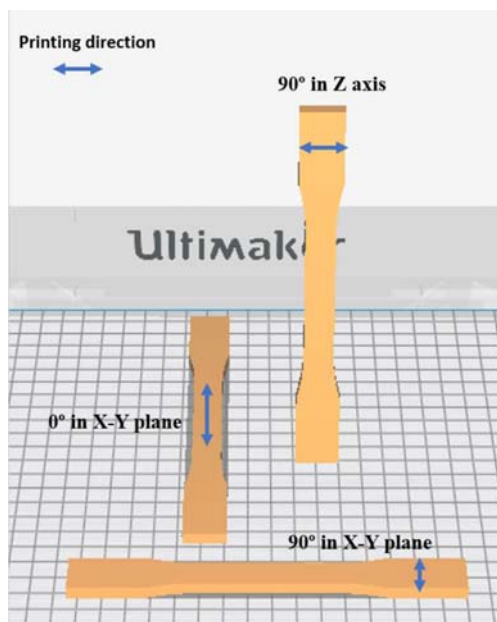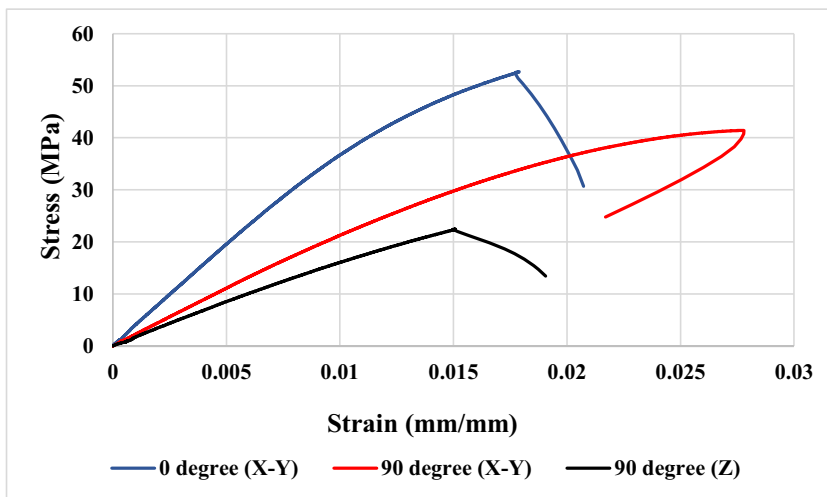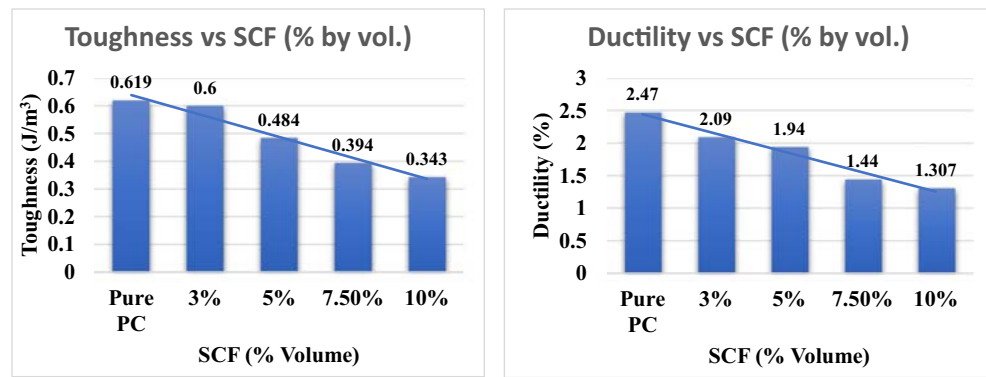

Fig. 12 Variation in Young's modulus at different SCF percentage at 0° in the X-Y plane, 90° in the X-Y plane, 90° in Z-axis

Fig. 13 Influence of SCF percentage on toughness and ductility of 3D-printed PC/SCF composite material

avoid them, all the cylindrical specimens were printed in 0° orientation. Compressive strength and compressive modulus were found from the stress-strain plot as shown in Fig. 17a. From Fig. 17b, we can conclude that the compressive strength and modulus increases as we increase the SCF percentage from 3 to 10% (by vol.). This increase was noticed because of good interlocking between the fibers and PC. Good interlocking has allowed the uniform distribution of load from the matrix to fibers. Although, the strength and modulus of PC/SCF composite material are lower than the pure PC. This

happened because of the occurrence of premature failure due to the formation of stress concentration at the fiber ends.

These local stresses may have been occurred due to local tension produced at the fiber tip. These stress concentrations result in the formation of microcracks and propagated towards the interface of fiber and the matrix resulting in weakening of strength and final failure. Brief analysis of the microstructural response of compression behavior of CM is shown in Fig. 16b, c. On the microstructural level, the figure indicates the cracks formation due to fiber overstressing under load.
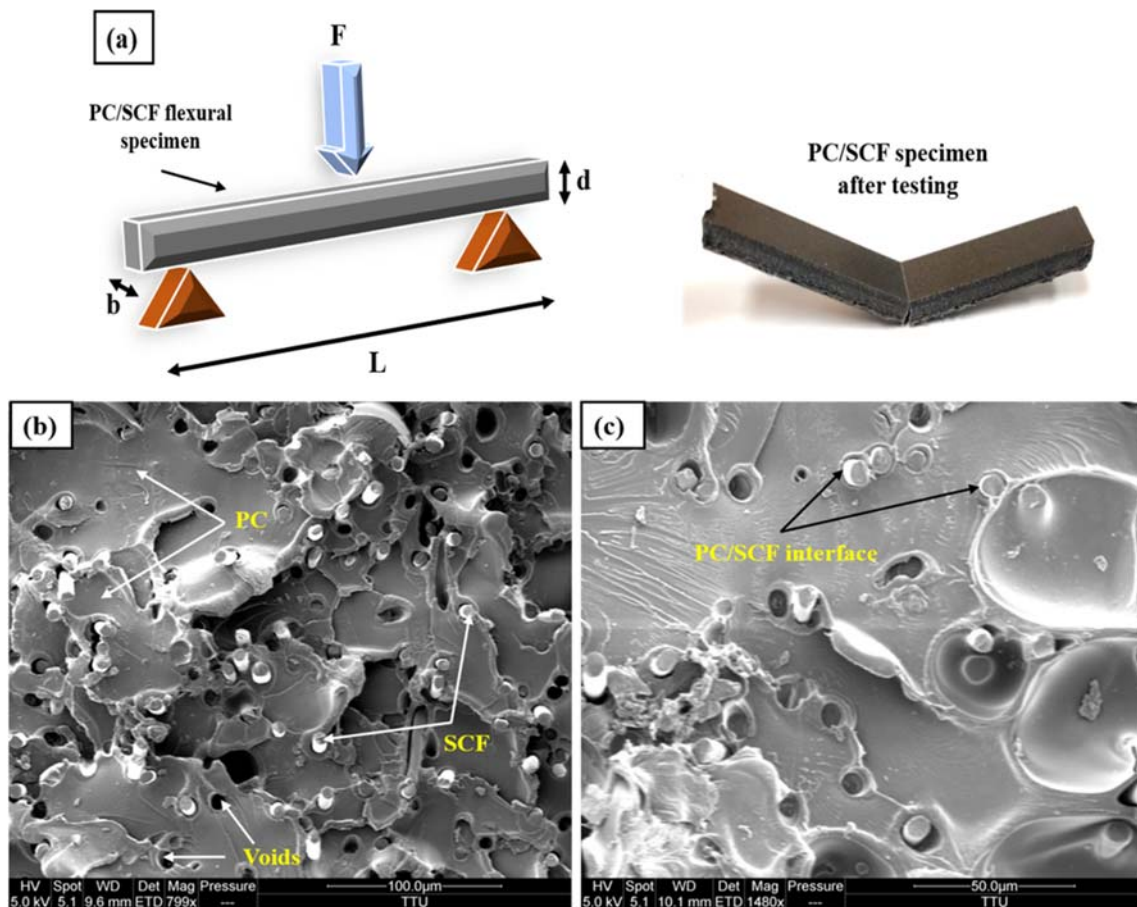

Fig. 14 a Schematic view of the flexural testing process and flexural specimen after testing. **b, c** SEM image of the flexural specimen after testing
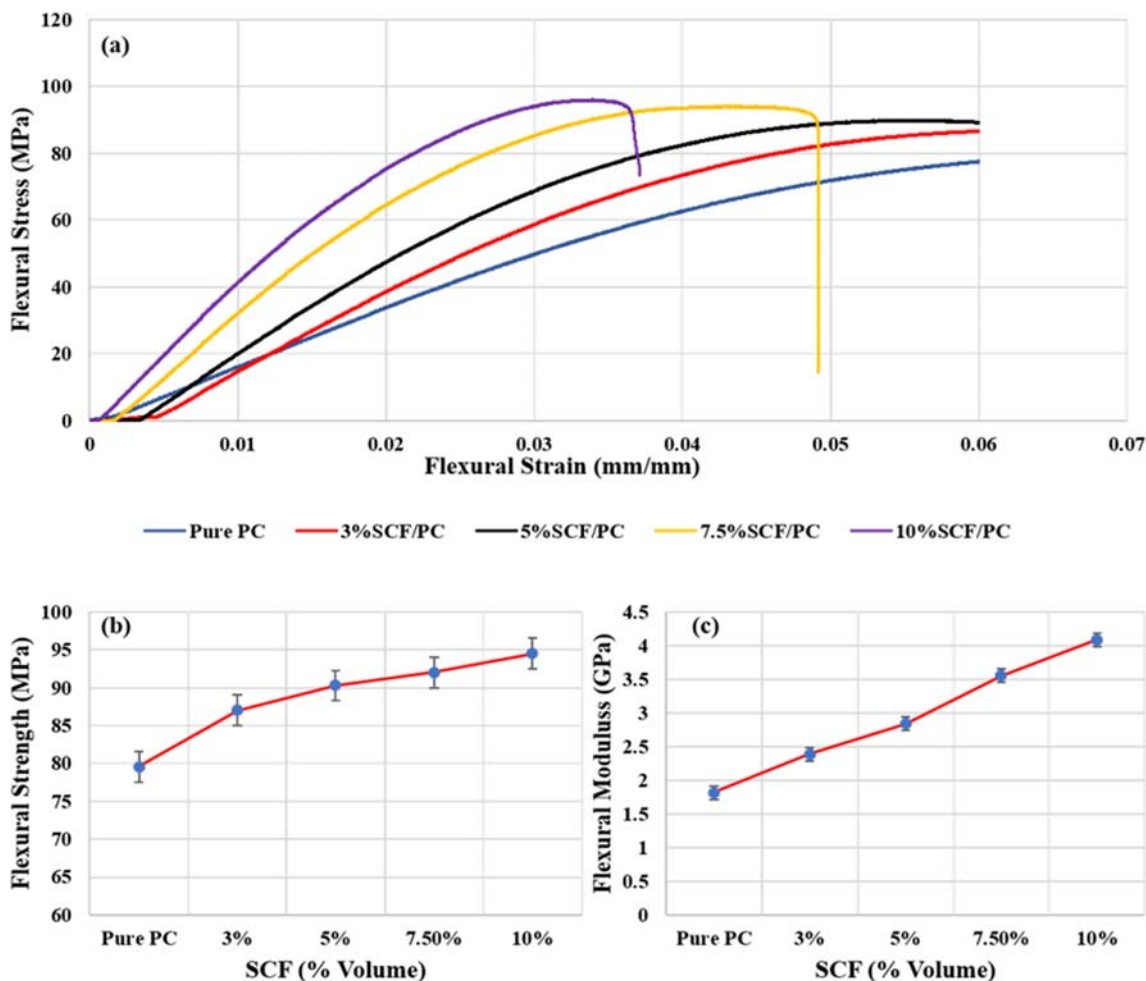
Fig. 15 a Flexural stress-strain curve for all SCF percentage. b Effect of SCF percentage on flexural strength. c Effect of SCF percentage on flexural modulus

3.5 Microhardness

Microhardness characterization was investigated using Buehler Digital Hardness Tester with a load of 50gf and dwell time of 30 s. Variation in the hardness values was noticed by varying the reinforcement value. Each 3D-printed specimen was indented at 10 positions at a distance of 10 μm [28]. The hardness values are measured using Eq. (5) [31] and average values were taken accordingly:

$$HV = 1 \cdot 8544 \frac{P}{d^2} \qquad (5)$$

where P (kgf) is the indenter load and d (mm) is length of the diagonal measured from one corner to another on the impression made by indenter. The microhardness values of SCF/PC polymer matrix composite increase as we increase SCF percentage, as expected as shown in Fig. 18. The maximum hardness value achieved was 160.8 MPa for the reinforcement concentration of 10%. (by vol.). This large increase in hardness values was noticed due to the uniform distribution of SCF inside the

matrix. Generally, polymer deforms when the load is applied, but the incorporation of high stiffness SCFs resists the deformation by providing the strong cross-linking between the polymer chains [32]. The increase is also noticed because the presence of SCF increases the brittleness in CM and ultimately decreases the indenter penetration on the surface of CM. All the above factors result in increasing the load-carrying capacity of CM and made it 2.09 times harder than pure PC.

4 Micromechanics and classical lamination theory

Micromechanics is the study of the behavior of the material at the fiber or matrix level. It helps us to predict the properties that are experimentally difficult to measure and also reduces the cost of experimental operations. In order to construct the micromechanical model for this study, empirical relations by Halpin and Tsai (Eqs. 6, 7, and 8) were used to predict the Young's modulus of the CM [33].
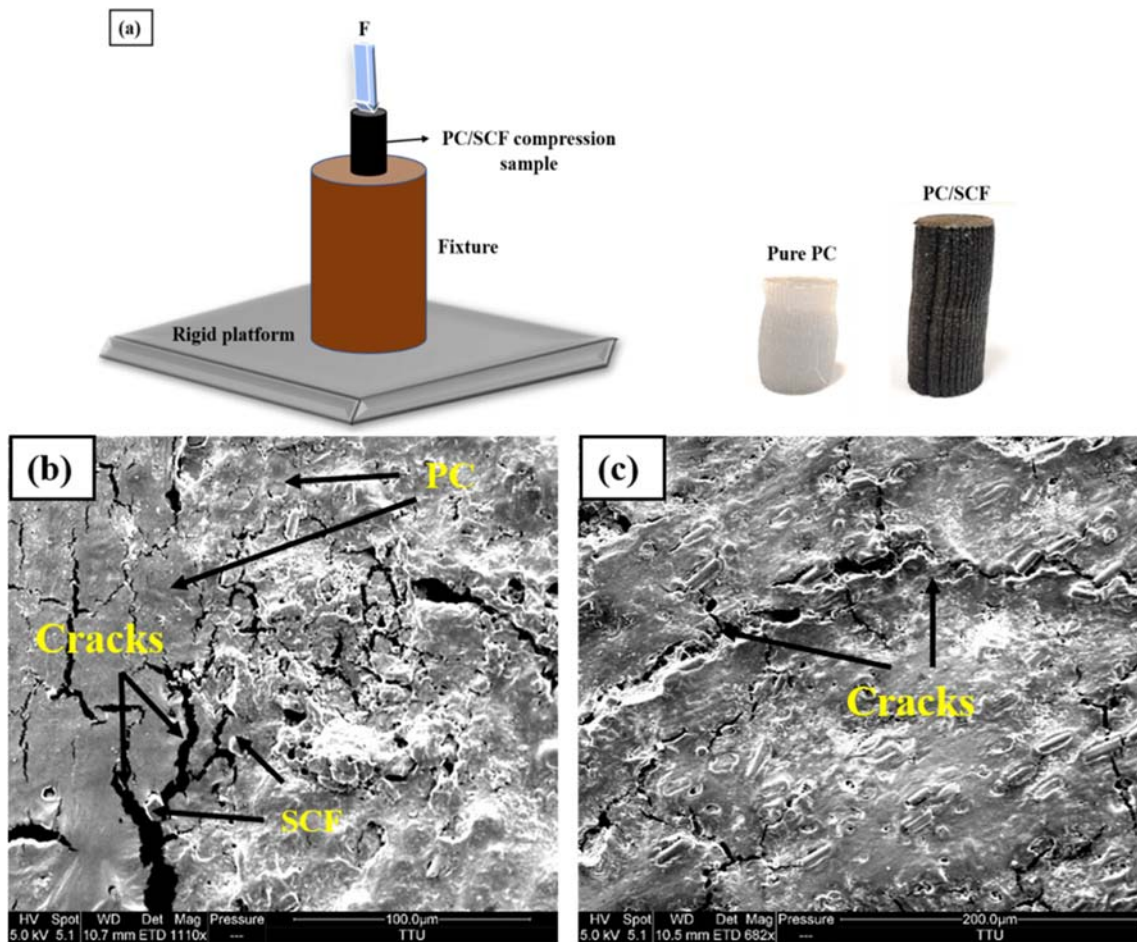
Fig. 16 **a** Schematic view of compression testing process and compression specimens after testing. **b, c** SEM image of compression specimen after testing

$$EL \text{ or } ET = \frac{Em(1 + \zeta*\eta L \text{ or } \eta T*Vf)}{1 - \eta L \text{ or } \eta T*Vf} \qquad (6)$$

$$\eta = \frac{\frac{Ef}{Em} - 1}{\frac{Ef}{Em} + \zeta} \qquad (7)$$

$$\zeta = 2*\text{Aspect ratio} \qquad (8)$$

Aspect ratio (AR) = length of fiber/diameter of fiber.

AR has no significant effect in the case of transverse properties and hence is considered as 1 in both the cases.

EL = Young's modulus of composite along the direction of the fiber, and ET = Young's modulus of composite in the direction perpendicular to the fiber.

ζ = measure of reinforcement and depends on the packing geometry, fiber geometry, and loading conditions. In this research, all the laminae were arranged in one direction and can be considered as balanced symmetric laminate. As their engineering properties are also known to us through the micromechanics approach,

it is easy to find the in-plane engineering constants from the ABD matrix [34].

The following assumptions should be considered before applying this approach [35].

1. Thickness of the laminate should be smaller than other dimensions
2. All the laminas are perfectly bonded to each other
3. Stresses and strains through the thicknesses should be negligible
4. Laminate and lamina are linearly elastic
5. No damage to laminate

Equation (9) shown below helps to define the elastic properties of the entire laminate [33].

$$\left(\frac{N}{M}\right) = \begin{bmatrix} A & B \\ B & D \end{bmatrix} * \left(\frac{\in}{k}\right) \qquad (9)$$

where N, M, A, B, D, $\in$, and k are resultant force, resultant moments, extensional stiffness matrix, coupling stiffness
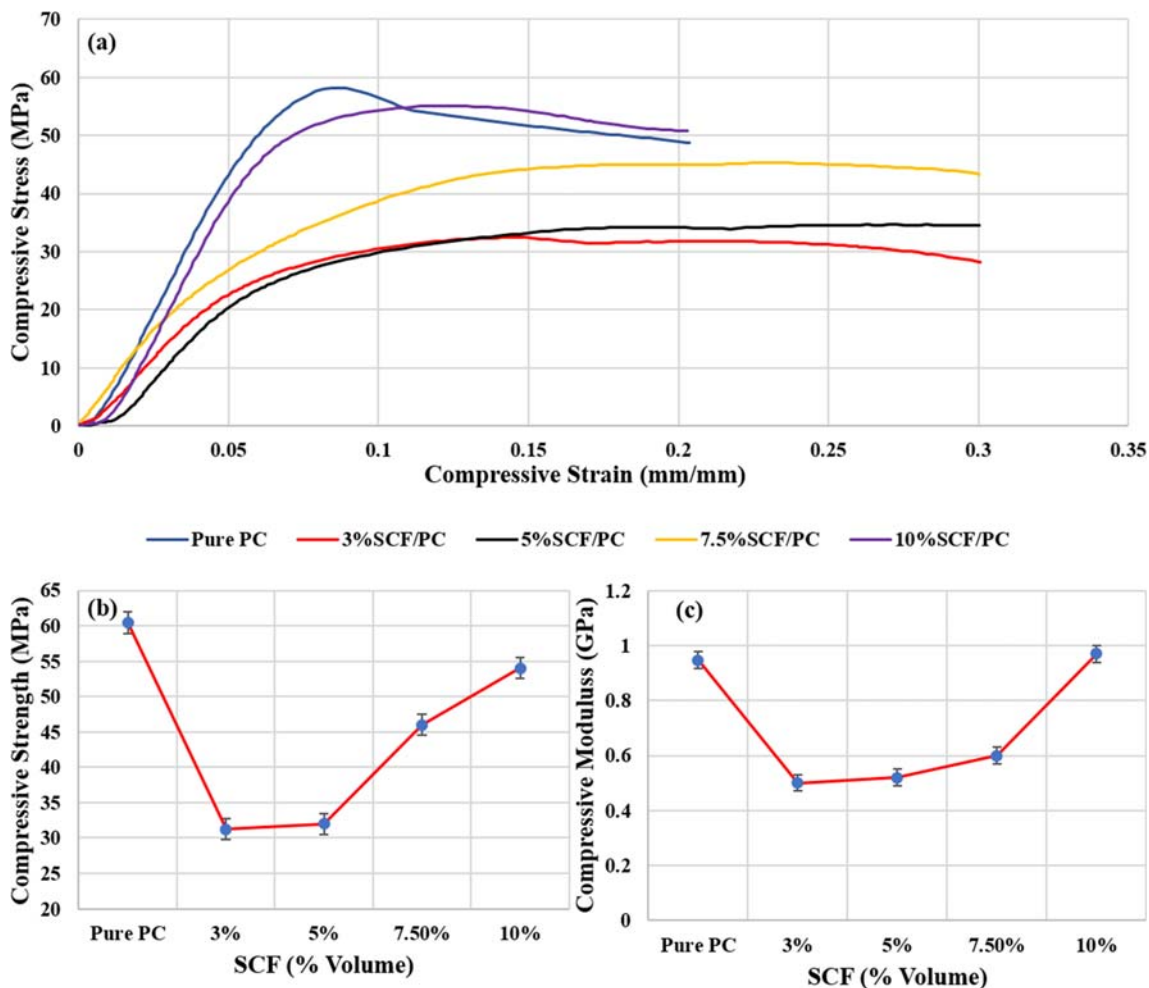
Fig. 17 **a** Compression stress-strain curve for all SCF percentage. **b** Effect of SCF percentage on compressive strength. **c** Effect of SCF percentage on the compressive modulus

matrix, bending stiffness matrix, midplane strain, and plate curvature, respectively. In this research, balanced symmetric laminate is considered which makes matrix B and A16 and A26 of matrix A be zero. Matrix D is also zero because of no applied moments. This reduces Eq. (9) to Eq. (10):

Fig. 18 Influence of SCF percentage on microhardness of 3D printed PC/SCF composite material

$$\begin{bmatrix} Nx \\ Ny \\ Nxy \end{bmatrix} = \begin{bmatrix} A11 & A12 & 0 \\ A21 & A22 & 0 \\ 0 & 0 & A66 \end{bmatrix} \begin{bmatrix} \in x \\ \in y \\ \gamma xy \end{bmatrix} \quad (10)$$

after considering constant strains throughout the thickness.

In order to find the modulus in X, Y, and X-Y-direction (Ex, Ey, Exy), resultant forces (Nx, Ny, Nxy) and strains ($\in x, \in y, \gamma xy$) need to be calculated:

$$Ex = \frac{\frac{Nx}{t}}{\in x}, \quad Ey = \frac{\frac{Ny}{t}}{\in y}, \quad Exy = \frac{\frac{Nxy}{t}}{\gamma xy} \quad (11)$$

Solving Eqs. (10) and (11) gives you the respective modulus of laminate shown in Eq. (12):

$$Ex = \frac{A11*A22 - A12*A12}{t*A22}, \quad Ey = \frac{A11*A22 - A12*A12}{t*A11} \quad (12)$$

Equation (13) is the empirical formula used to predict the young's modulus of CM reinforced with fibers and are randomly oriented [33]:

$$Erandom = \left(\frac{3}{8}\right)Ex + \left(\frac{5}{8}\right)Ey \qquad (13)$$

A comparison between the experimental and analytical results is shown in Fig. 19. The errors occurred due to the formation of inter-bead voids during the 3D printing process. From the results, we can also observe that as we increase the SCF percentage inside the CM, errors in Young's modulus values start decreasing.

5 Statistical analysis

Statistical analysis allows us to study the influence of input variables on the entire process. Study of input parameters one at a time and their interactions is an efficient way to extract the meaningful behavior of the independent variables (printing direction, SCF percentage, and printing speed) on the dependent variables (Longitudinal and transverse tensile strength, and Young's modulus).

5.1 Analysis of variance

ANOVA analysis was performed on the tensile strength and modulus data obtained after printing in the longitudinal and transverse direction. The analysis was done to investigate the influence of individual input parameters and their interactions on the final mechanical properties. The ANOVA model chosen is shown in Eq. (14) [36]:

$$Y_{ijk} = \mu.. + \alpha_i + \beta_j + (\alpha\beta)_{ij} + (\alpha\gamma)_{ik} + (\beta\gamma)_{jk} + \varepsilon_{ijk} \qquad (14)$$

$\mu..$ is a constant (overall mean), α_i is the main effect for factor A (orientation) at the ith level, β_j is the main effect for factor B (concentration) at the jth level, γ_k is the main effect for factor C (printing speed) at the kth level, and $(\alpha\beta)_{ij}$, $(\alpha\gamma)_{ik}$, and $(\beta\gamma)_{jk}$ are the interaction effects. The probability value (p value) helps to determine whether the input variable is significant or not by comparing it with the alpha value of 0.05. If the p value is smaller than 0.05, the input variable is considered to be significant. Table 6 shows the ANOVA results for tensile strength and modulus. Printing direction, reinforcement, and printing speed all have the p values less than 0.05 making them significant factors for the cases of strength and modulus. Two-way interaction of reinforcement concentration with the other factors is also considered to be significant. So, ANOVA analysis concluded that printing direction and reinforcement concentration have created a most significant influence on the strength and modulus as compared to printing speed.

5.2 Response surface methodology

RSM was performed to optimize the processing parameters of experimental methods opted to 3D print the PC/CF CM [36]. It also helps us to get the idea for the input parameters or combination of input parameters that provides us the

Fig. 19 Young's modulus comparison for analytical and experimental approach
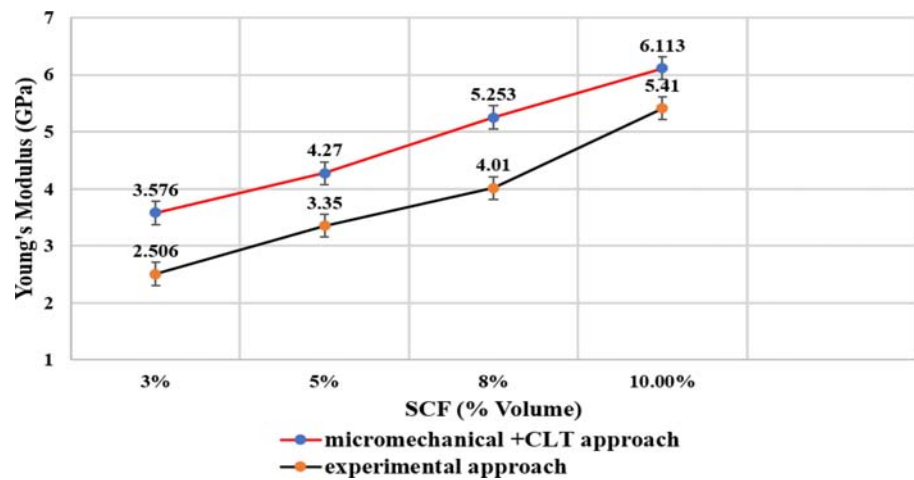
SCF (% by vol.)	Young's modulus (GPa)		
	Micromechanics + CLT	Experimental	Error (%)
3	3.576	2.506	42.69
5	4.27	3.35	27.46
7.5	5.253	4.01	30.99
10	6.113	5.41	12.99

Table 6 ANOVA of tensile strength and modulus and their interaction showing p values

Variables	DOF	Sum squares	Mean squares	F-value	p value
For tensile strength					
Orientation	1	226.3	2.26	7.978	0.009868
Concentration	1	524.7	5.25	18.501	0.000289
Printing speed	1	160.1	1.60	5.646	0.026627
Two-way interactions					
Orientation: concentration	1	99.9	99.9	3.523	0.073857
Orientation: printing speed	1	32.1	32.1	1.131	0.299065
Concentration: printing speed	1	176.8	176.8	6.233	0.020523
For Young's modulus					
Orientation	1	11.004	11	130.591	1.01E-10
Concentration	1	5.037	5.04	59.78	1.03E-07
Printing speed	1	0.75	0.75	8.901	0.00685
Two-way interactions					
Orientation: concentration	1	5.936	5.94	70.452	2.64E-08
Orientation: printing speed	1	0.001	0.001	0.007	0.93627
Concentration: printing speed	1	0.925	0.925	10.98	0.00316

maximum tensile strength and tensile modulus in 0° X-Y and 90° X-Y directions. The optimized model for RSM is shown in Eq. (15) [36]:

$$y = \beta_0 + \beta_1 x_1 + \beta_2 x_2 + \beta_{12} x_1 x_2 + \beta_{11} x_1^2 + \beta_{22} x_2^2 + \varepsilon \qquad (15)$$

where y is the response of the process, x_n is independent variables called factors, β_0 is constant-coefficient, β_1, β_2 are linear coefficients, β_{11}, β_{22} are quadratic coefficients, and β_{12} is the coefficient of the interaction. From the RSM results shown in Table 7 for the case of tensile strength, we can observe that both reinforcement and printing speed have p values less than 0.05 making them the significant parameter in deciding the TS.

Interaction between the speed and SCF% also creates a considerable influence on the outputs. Figure 20 shows the response surface plots for tensile strength and modulus, in order to get the optimized values. Optimum values of independent variables for tensile strength are shown in Table 7. Printing the PC reinforced with 6% (by vol.) SCF and 28 mm/s printing speed results in achieving the maximum strength for the final CM.

In the case of RSM analysis for modulus, only reinforcement concentration has a p value less than 0.05 making it a statistically significant parameter. Optimum values are shown in Table 8, which indicates that CM printing with 1.25% (by vol.) SCF and 53 mm/s speed results in obtaining the significant modulus for the final part.

Table 7 RSM of tensile strength and modulus and their interaction showing p values

| Variables	Estimate	Standard error	t-value	p value
For tensile strength				
Concentration	− 6.0546	1.4329	− 4.2255	0.000321
Printing speed	− 2.7438	1.2183	− 2.2521	0.034162
Concentration: printing speed	− 4.2839	1.7549	− 2.4412	0.022752
For Young's modulus				
Concentration	0.5885	0.1432	4.1097	0.00042
Printing speed	− 0.18745	0.12176	− 1.54	0.13731
Concentration: printing speed	− 0.30992	0.17538	− 1.77	0.09046
Tensile strength: Young's modulus				
Concentration	− 2.73304	0.97908	− 2.7914	0.007281
Printing speed	− 1.46564	0.83248	− 1.7606	0.08408
Concentration: printing speed	− 2.29689	1.19908	− 1.9155	0.060825
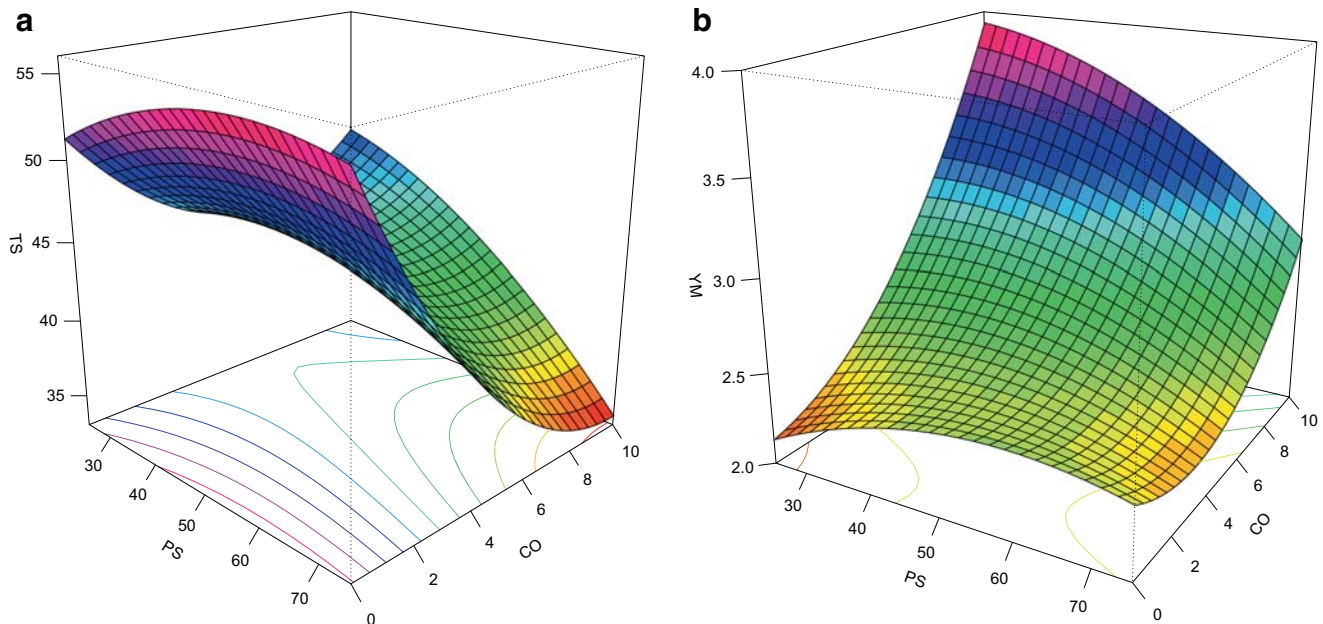
Fig. 20 Plots showing the variation of dependent variables w.r.t to independent variables for tensile strength and modulus

6 Conclusions

The paper has presented a brief discussion on 3D-printed PC reinforced with SCF composite material using the FFF technique. Fabrication, mechanical characterization, and surface micrography of specimens with the change in orientation (0° in the X-Y plane, 90° in the X-Y plane, and 90° in the Z-axis), SCF volume fractions and printing speed were deeply analyzed and reported in this article. On the basis of analysis, the following conclusions have been drawn:

- SCF is distributed uniformly inside the PC matrix with fewer gaps at the interface indicating good adhesion between the polymer and fibers.
- Bead-to-bead and then layer-by-layer stack-up of CM leads to an orthotropic behavior of the final part.
- Tensile strength and modulus show a significant increase with the increase in SCF concentration up to 7.5% (by vol.) but 4% less than the pure PC due to the formation of local stresses produced by the imperfect alignment of short fibers. The maximum strength and modulus achieved are 52.68 MPa and 5.41 GPa respectively. Higher percentages show a decrease in mechanical

properties because of fiber breakage, fiber accumulation, and fiber pullout.
- Flexural strength and modulus increase with an increase in fiber reinforcement. The maximum strength and modulus achieved are 94.5 MPa and 4.085 GPa respectively which is higher than the tensile properties of printed samples.
- Compressive strength and modulus also increase with an increase in fiber percentage from 3 to 10% but not more than the pure PC because of the crack formation due to fiber overstressing under the load. The maximum strength and modulus achieved are 54 MPa and 0.97 GPa respectively.
- The maximum hardness value observed is 160.8 MPa at the fiber percentage of 10% (by vol.).
- Mechanical properties were also calculated using the micromechanics approach and classical lamination theory (CLT) and compared with experimental results found for longitudinal tensile modulus. After comparison, a decent agreement was observed at higher SCF percentage
- Printing orientation and SCF percentage are the most influential parameters for the fabrication of composite material. ANOVA analysis also stated that the combination of SCF percentage with printing direction and speed has also created a significant effect on the final mechanical performance of the parts.
- Parameter setting with fiber percentage of 5.789% (by vol.) and printing speed of 29.992 mm/s is found out the be optimized values for better mechanical properties

Table 8 Optimum values obtained after RSM analysis

Variables	SCF concentration	Printing speed
Tensile strength	6.087	28.125
Young's modulus	1.254	53.035
Tensile strength: Young's modulus	5.789	29.992

References

1. Nasirov A, Fidan I (2020) Prediction of mechanical properties of fused filament fabricated structures via asymptotic homogenization. Mech Mater 145:103372. https://doi.org/10.1016/j.mechmat.2020.103372

2. Yasa E, Ersoy K (2018) A review on the additive manufacturing of fiber reinforced polymer matrix composite. Solid Free Fabr Symp. 1024–1033. https://sffsymposium.engr.utexas.edu/sites/default/files/2018/084%20AReviewontheAdditiveManufacturingfFiberRe.pdf

3. Ahn SH, Montero M, Odell D et al (2002) Anisotropic material properties of fused deposition modeling ABS. Rapid Prototyp J. https://doi.org/10.1108/13552540210441166

4. Moritz T, Maleksaeedi S (2018) Additive manufacturing of ceramic components. In: Additive manufacturing. https://doi.org/10.1016/b978-0-12-812155-9.00004-9

5. Melchels FPW, Feijen J, Grijpma DW (2010) A review on stereolithography and its applications in biomedical engineering. Biomaterials. https://doi.org/10.1016/j.biomaterials.2010.04.050

6. Kruth JP, Mercelis P, Van Vaerenbergh J et al (2005) Binding mechanisms in selective laser sintering and selective laser melting. Rapid Prototyp J. https://doi.org/10.1108/13552540510573365

7. Fidan I, Imeri A, Gupta A, Hasanov S, Nasirov A, Elliott A, Alifui-Segbaya F, Nanami N (2019) The trends and challenges of fiber reinforced additive manufacturing. Int J Adv Manuf Technol 102: 1801–1818. https://doi.org/10.1007/s00170-018-03269-7

8. Goh GD, Yap YL, Agarwala S, Yeong WY (2019) Recent Progress in additive manufacturing of fiber reinforced polymer composite. Adv Mater Technol 4:1–22. https://doi.org/10.1002/admt.201800271

9. Hofstätter T, Pedersen DB, Tosello G, Hansen HN (2017) Applications of fiber-reinforced polymers in additive manufacturing. Procedia CIRP 66:312–316. https://doi.org/10.1016/j.procir.2017.03.171

10. Rezaei F, Yunus R, Ibrahim NA (2009) Effect of fiber length on thermomechanical properties of short carbon fiber reinforced polypropylene composites. Mater Des 30:260–263. https://doi.org/10.1016/j.matdes.2008.05.005

11. Yi H, Qi L, Luo J, Li N (2019) Hole-defects in soluble core assisted aluminum droplet printing: metallurgical mechanisms and elimination methods. Appl Therm Eng. https://doi.org/10.1016/j.applthermaleng.2018.12.013

12. Lu ZL, Lu F, Cao JW, Li DC, Lian YY, Miao K, Jing H (2013) Fabricating hollow turbine blades using short carbon fiber-reinforced SiC composite. Int J Adv Manuf Technol 69:417–425. https://doi.org/10.1007/s00170-013-5049-z

13. Jiang J, Ren Z, Ma Z et al (2020) Mechanical properties and microstructural evolution of TA15 Ti alloy processed by selective laser melting before and after annealing. Mater Sci Eng A. https://doi.org/10.1016/j.msea.2019.138742

14. Ma Z, Zhang DZ, Liu F et al (2020) Lattice structures of Cu-Cr-Zr copper alloy by selective laser melting: microstructures, mechanical properties and energy absorption. Mater Des. https://doi.org/10.1016/j.matdes.2019.108406

15. Qi L, Yi H, Luo J et al (2020) Embedded printing trace planning for aluminum droplets depositing on dissolvable supports with varying section. Robot Comput Integr Manuf. https://doi.org/10.1016/j.rcim.2019.101898

16. Thomas DJ (2018) Developing nanocomposite 3D printing filaments for enhanced integrated device fabrication. Int J Adv Manuf Technol 95:4191–4198. https://doi.org/10.1007/s00170-017-1478-4

17. Imeri A, Fidan I, Allen M, Wilson DA, Canfield S (2018) Fatigue analysis of the fiber reinforced additively manufactured objects. Int J Adv Manuf Technol 98:2717–2724. https://doi.org/10.1007/s00170-018-2398-7

18. Ferreira RTL, Amatte IC, Dutra TA, Bürger D (2017) Experimental characterization and micrography of 3D printed PLA and PLA reinforced with short carbon fibers. Compos Part B Eng 124:88–100. https://doi.org/10.1016/j.compositesb.2017.05.013

19. Zhong W, Li F, Zhang Z et al (2001) Short fiber reinforced composites for fused deposition modeling. Mater Sci Eng A. https://doi.org/10.1016/S0921-5093(00)01810-4

20. Ivey M, Melenka GW, Carey JP, Ayranci C (2017) Characterizing short-fiber-reinforced composites produced using additive manufacturing. Adv Manuf Polym Compos Sci 3:81–91. https://doi.org/10.1080/20550340.2017.1341125

21. Tekinalp HL, Kunc V, Velez-Garcia GM, Duty CE, Love LJ, Naskar AK, Blue CA, Ozcan S (2014) Highly oriented carbon fiber-polymer composites via additive manufacturing. Compos Sci Technol 105:144–150. https://doi.org/10.1016/j.compscitech.2014.10.009

22. Sedighi I, Ayatollahi MR, Bahrami B et al (2019) Mechanical behavior of an additively manufactured poly-carbonate specimen: tensile, flexural and mode I fracture properties. Rapid Prototyp J. https://doi.org/10.1108/RPJ-03-2019-0055

23. Kumar M, Ramakrishnan R, Omarbekova A (2019) 3D printed polycarbonate reinforced acrylonitrile–butadiene–styrene composites: composition effects on mechanical properties, micro-structure and void formation study. J Mech Sci Technol 33:5219–5226. https://doi.org/10.1007/s12206-019-1011-9

24. Rezaei F, Yunus R, Ibrahim NA, Mahdi ES (2008) Development of short-carbon-fiber-reinforced polypropylene composite for car bonnet. Polym-Plast Technol Eng. https://doi.org/10.1080/03602550801897323

25. Rajak DK, Pagar DD, Menezes PL, Linul E (2019) Fiber-reinforced polymer composites: manufacturing, properties, and applications. Polymers (Basel). https://doi.org/10.3390/polym11101667

26. Agarwal BD, Broutman LJ, Bert CW (1981) Analysis and performance of fiber composites. J Appl Mech. https://doi.org/10.1115/1.3157582

27. Misra S, Hussain M, Gupta A et al (2019) Fabrication and characteristic evaluation of direct metal laser sintered SiC particulate reinforced Ti6Al4V metal matrix composites. J Laser Appl. https://doi.org/10.2351/1.5086982

28. Gupta A, Hussain M, Misra S et al (2018) Processing and characterization of laser sintered hybrid B4C/cBN reinforced Ti-based metal matrix composite. Opt Lasers Eng. https://doi.org/10.1016/j.optlaseng.2018.01.015

29. Forster AM (2015) Materials testing standards for additive manufacturing of polymer materials: state of the art and standards applicability. In: additive manufacturing materials: standards, testing and applicability. National Institute of Science and Technology 20. https://doi.org/10.6028/NIST.IR.8059

30. ASTM D695–15 (2008) Standard test method for compressive properties of rigid plastics. ASTM Int. https://doi.org/10.1520/D0695-10.2

31. Broitman E (2017) Indentation hardness measurements at macro-, micro-, and nanoscale: a critical overview. Tribol Lett. https://doi.org/10.1007/s11249-016-0805-5

32. Mohamed YS, El-Gamal H, Zaghloul MMY (2018) Microhardness behavior of fiber reinforced thermosetting composites embedded with cellulose nanocrystals. Alexandria Eng J 57:4113–4119. https://doi.org/10.1016/j.aej.2018.10.012

33. Agarwal BD, Broutman LJ, Chandrashekhara K (2006) Analysis and performance of fiber composites third edition. 132–281. https://doi.org/10.1115/1.3157582

34. Nasirov A, Hasanov S, Fidan I (2019) Prediction of mechanical properties of fused deposition modeling made parts using multiscale modeling and classical laminate theory. In: Proceedings

of the 30th Annual International Solid Freeform Fabrication Symposium-An Additive Manufacturing Conference, Austin, TX, 1376. https://www.researchgate.net/publication/338172358

35. Nettles AT (1994) Basic Mechanics of laminated composite plates. NASA Ref pulication. https://ntrs.nasa.gov/search.jsp?R=19950009349

36. Barnett V, Neter J, Wasserman W (1975) Applied linear statistical models. J R Stat Soc Ser A. https://doi.org/10.2307/2984653